American Mineralogist, Volume 92, pages 44–56, 2007

Speciation of Fe in silicate glasses and melts by in-situ XANES spectroscopy

Max Wilke,[1,*] François Farges,[2,3] Georg M. Partzsch,[4] Christian Schmidt,[5] and Harald Behrens[6]

[1]Institut für Geowissenschaften, Universität Potsdam, Postfach 601553, D-14415 Potsdam, Germany
[2]Laboratoire des Géomateriaux, Université de Marne-la-Vallée, F-77454 Marne-la-Vallée cedex 2, France
[3]Department of Geological and Environmental Sciences, Stanford University, Stanford, California 94305, U.S.A.
[4]Mineralogisches Institut, Universität Heidelberg, INF 236, D-69120 Heidelberg, Germany
[5]GeoForschungsZentrum Potsdam, Telegrafenberg, D-14473 Potsdam, Germany
[6]Institut für Mineralogie, Universität Hannover, D-30167 Hannover, Germany

Abstract

In-situ X-ray absorption spectroscopy at the Fe *K*-edge was used to characterize the local structural environment of Fe^{2+} and Fe^{3+} in silicate melts at high temperature (up to 1050 °C) in comparison to their quenched glassy analog at room temperature. Measurements were performed on binary alkali-silicate compositions and on haplogranitic compositions, which were doped with about 5 wt% Fe_2O_3. Changes in the structural environment of Fe were evaluated by analyzing both the pre-edge feature and the first maximum of the EXAFS of the spectra. In most cases, the spectra collected at high temperature differed from those of the quenched samples. At reducing conditions, the melts showed slightly higher amounts of low-coordinated Fe^{2+} than their glassy counterparts. This finding is consistent with results of earlier studies (e.g., Jackson et al. 1993), but the observed change in speciation is smaller than reported by these authors. At oxidizing conditions, glasses and melts displayed a more heterogeneous behavior. The spectra of alkali-silicate compositions indicate higher amounts of low-coordinated Fe^{3+} in the melt, whereas no significant difference between melt and glass was observed for Fe^{3+} in haplogranitic compositions, even if the latter are peralkaline. The amount of non-bridging O atoms in the glass/melt system appears to play an important role particularly for Fe^{3+}. However, more complex relationships between Fe and other structural components, especially Al, are possible.

Keywords: XAS (XAFS, XANES), Fe *K*-edge, high-temperature studies, Fe in silicate melts, melt properties, glass properties

Introduction

In magmatic systems, Fe is the most abundant transition element. Due to its heterovalent nature and the different crystal-chemical behavior of the reduced and oxidized species, Fe affects a wide number of physical and chemical properties of magmas, such as density, viscosity, stability of phases, and nucleation during crystallization (e.g., Dingwell and Brearley 1988; Dingwell 1989; Lange and Carmichael 1990; Toplis and Carroll 1995; Liebske et al. 2003; Liu and Lange 2006). Particularly, the viscosity of Fe-bearing silicate melts decreases considerably with decreasing Fe^{3+}-content of the melt (e.g., Dingwell and Virgo 1987; Dingwell 1989, 1991; Liebske et al. 2003; Bouhifd et al. 2004), which provides clear but indirect evidence for differences in the structural role of Fe^{3+} and Fe^{2+}. Many studies have addressed the structural role of Fe in melts using glasses as a structural analog (e.g., Calas and Petiau 1983; Virgo and Mysen 1985; Alberto et al. 1996; Mysen et al. 1985; Hannoyer et al. 1992; Rossano et al. 1999, 2000; Burkhard 2000; Galoisy et al. 2001; Giuli et al. 2002). The structural role of Fe^{3+} in silicate melts is considered to be similar to that of Al. Thus, in most cases, Fe^{3+} was assigned to tetrahedral site geometry, although evidence for higher coordination was also found, especially at low Fe^{3+} contents (e.g., Hannoyer et al. 1992; Farges et al. 2004). Very recently, results of an investigation on the partial molar volume of Fe_2O_3 in alkali-silicate melts were taken as an argument for fivefold-coordinated Fe^{3+} (Liu and Lange 2006). On the other hand, Fe^{2+} is distributed over sixfold-, fivefold-, and fourfold-coordinated sites in silicate glasses, with the last two dominating (e.g., Rossano et al. 2000). The observation of fourfold (i.e., tetrahedral) Fe^{2+} has been taken as evidence for a network-forming role of Fe^{2+} (Waychunas et al. 1988; Jackson et al. 1993). However, a network-forming behavior of Fe^{2+} is in conflict with viscosity data. In addition, the network-modifying role of Fe^{2+} via redox-dependent changes in the polymerization of the samples was clearly shown using Raman spectroscopy (Wang et al. 1993).

Based on heat capacity and configurational entropy arguments (e.g., Richet and Bottinga 1995), the structure of melts close to the temperature of glass transformation (T_g) is usually considered to be relatively close to the one at higher temperature. Thus, the structure of the glass, which is frozen-in at the transformation, is considered to represent the one found in the melt. However, there is evidence for structural changes close to T_g around transition elements even at high quench rates (Waychunas et al. 1988; Jackson et al. 1993 for Fe^{2+}; Farges et al. 1994 for Ni). Farges and Brown (1996) summarized these observations by correlating

* E-mail: max@geo.uni-potsdam.de

the change in speciation at T_g to the average thermal expansion of the bonds around the cation and relating this to the bond valence of the transition element at room temperature. Divalent transition elements are predicted to show much more coordination changes at T_g for a given composition than higher-charged cations such as Ti (Farges et al. 1996) or Si and Al (Stebbins and Farnan 1992; Stebbins 1995). Thus, structural relaxations during the quench process may obscure the structural changes occurring at higher temperatures, so that the glass is potentially not structurally representative of the molten state. The effect of the quench process on the analysis of the melt structure can be minimized by combining spectroscopic and molecular dynamic simulation techniques, as shown by Rossano et al. (2000) and Farges et al. (2004). Despite the intrinsic limitations of these simulations (ultra fast quench), they provide important constraints for the interpretation of spectroscopic data obtained on quenched samples. Still, a direct observation of the element speciation under in-situ conditions is the most desirable and reliable source of information. In-situ studies of Fe^{2+} using X-ray absorption fine-structure (XAFS) spectroscopy (Waychunas et al. 1988; Jackson et al. 1993) provided evidence for a strong increase of low-coordinated Fe^{2+} above T_g (compared to the glassy state). However, that finding was mainly based on information from the pre-edge feature of spectra that were normalized inappropriately (i.e., to the maximum in the region near the edge, i.e., the XANES). The height of the XANES maximum is affected significantly by thermally induced anharmonicity and thus, the ratio of the pre-edge intensity to the XANES maximum is a function of the temperature. Therefore, the reported changes in the pre-edge do not necessarily reflect real structural changes. Furthermore, the pre-edge feature probes the symmetry of the Fe site, which might change as a function of temperature while the coordination number remains constant. Another in-situ method, Raman spectroscopy, was utilized to study Fe-bearing Na-silicate glass and melt (Wang et al. 1993). However, no direct investigation of the local structure around Fe in the melt was made, i.e., the Fe-coordination was deduced only from room-temperature Mössbauer spectra after quenching the sample.

In the study presented here, we have investigated the local structural environment of Fe in silicate glass and melt by using XAFS methods. XAFS is sensitive to oxidation state and provides structural information on the nearest and next-nearest atoms around the absorbing atom (Brown et al. 1995). The XANES region near the edge, especially the pre-edge feature located ~15–20 eV before the main *K*-edge crest of Fe, is sensitive to the oxidation state (e.g., Waychunas et al. 1983; Wu et al. 1999; Wilke et al. 2001; Berry et al. 2003). In addition, XANES provides information on the first coordination shell around Fe, because the contributions arising from next-nearest neighbors are small in glasses and melts (Bugaev et al. 2005). Thus, differences in the symmetry and the coordination of Fe between glasses and melts will be reflected in the pre-edge and in the fine structure of the XANES.

Waychunas et al. (1988) and Jackson et al. (1993) studied only Fe^{2+} in melts and glasses. In this study, we provide new information on the incorporation of Fe^{2+} and Fe^{3+} into a variety of binary alkali-silicate as well as in haplogranitic compositions in the system SiO_2(Qz)-$NaAlSi_3O_8$(Ab)-$KAlSi_3O_8$(Or). These investigations are used to further constrain the relationship between Fe speciation and bulk composition, focusing particularly on the influence of NBO/T, the number of non-bridging oxygen atoms per tetrahedron (Mysen 1988). We used a more appropriate normalization procedure for the XANES region, which is based on a large energy range (about 250 eV in total) before and after the Fe *K*-edge. The interpretation of the spectra of the glasses and melts was evaluated using spectra of crystalline materials that were recorded at various temperatures.

Experimental methods

Starting materials

The Fe-free starting materials were synthesized from mixtures of powdered dry oxides (SiO_2, Al_2O_3) and carbonates ($CaCO_3$, Na_2CO_3, and K_2CO_3). The mixtures were decarbonated by stepwise heating to 1050 °C in a Platinum-crucible and annealed for about 0.5 h. After this first step, the haplogranitic composition ($Qz_{44}Ab_{26}Or_{30}$, Qz: SiO_2, Ab: $NaAlSi_3O_8$, Or: $KAlSi_3O_8$) was equilibrated at 1600 °C for two days in air, quenched and crushed, and annealed again for another 3 days. Iron was added to aliquots of the crushed base glass and the mixture was remelted for another two days. The peralkaline haplogranitic composition was produced by adding Na_2CO_3 to aliquots of the Fe-bearing $Qz_{44}Ab_{26}Or_{30}$ glass and annealing for another day. The alkali-silicate compositions were annealed at 1300 °C for 1 hour to minimize loss of alkalis. Again, Fe was added in a second step followed by further equilibration. The resulting glasses were checked for homogeneity and composition using an electron microprobe. Electron microprobe analyses were conducted using a CAMECA SX100 (GFZ Potsdam) and a JEOL 8800 (Museum für Naturkunde, Berlin). The glasses were analyzed with an acceleration voltage of 15 kV, a beam current of 15 nA, and a beam diameter enlarged to 20 µm. The counting times were 10 s on the peaks and 5 s on the background.

One major difference in the bulk structure of the alkali-silicates and the haplogranitic compositions is the degree of polymerization. The nominal NBO/T calculated for the Fe-free compositions is about 2/3 for the alkali-silicate glasses, 0 for the haplogranite, and 0.1 for the peralkaline haplogranite. Due to a slight excess of Al over the alkalis in the haplogranite, a negative NBO/T value is calculated for the Fe-free haplogranite (see Table 1). This value has no physical relevance and may thus be taken as a formal NBO/T. The procedure for calculating NBO/T suggested by Mysen (1988) does not account for excess Al, which is mainly due to uncertainties in the structural role of Al in such a case. Addition of Fe will change the NBO/T ratio, depending on the oxidation state. Based on the assignment of Mysen (1988), Fe^{2+} will increase and Fe^{3+} will decrease NBO/T. This will, likewise, yield a negative value for the Fe^{3+}-bearing haplogranitic composition. The NBO/T ratio of the alkali silicate compositions calculated from the microprobe analyses also differs from the nominal value, which is due to some deficiency in the alkali content that lowers the alkali/Si ratio.

Table 1. Composition (wt%) of starting glasses (with their standard deviation in parenthesis) together with calculated CIPW-normative components and NBO/T

	AOQ	AOQNA	NS3	KS3
SiO_2	76.58(27)	73.96(43)	71.80(78)	63.58(84)
Al_2O_3	10.71(21)	10.00(32)		
K_2O	4.68(10)	4.30(09)		29.01(77)
Na_2O	2.82(11)	7.41(18)	23.19(56)	
Fe_2O_3 (tot.)	4.25(13)	4.71(14)	4.43(34)	5.89(57)
Total	99.04	100.38	99.42	98.48
Qz	44.6	36.2	n.a.	n.a.
Ab	29.2	28.7	n.a.	n.a.
Or	29.6	26.5	n.a.	n.a.
C	1.00	0.00	n.a.	n.a.
NS	0.00	8.16	n.a.	n.a.
NBO/T (Fe-free)	–0.013	0.094	0.626	0.582
NBO/T (Fe^{2+})	0.058	0.177	0.719	0.721
NBO/T (Fe^{3+})	–0.047	0.051	0.554	0.479

Note: n.a. = not applicable.

XANES

High-resolution XANES spectra at the Fe *K*-edge were collected at the Hamburger Synchrotronstrahlungslabor (HASYLAB, Hamburg, Germany) on the bending-magnet beamline A1. The storage ring operating conditions were 4.5 GeV positron energy and 80–140 mA positron current. An Si (111) four-crystal monochromator was used, providing an energy resolution $E/\Delta E = 12\,200$ or 0.5 eV at 6 keV (Attenkofer et al. 2000). This energy resolution is significantly smaller than the finite core-hole lifetime width of the absorbing element (about 1.25 eV at the Fe *K*-edge; Krause and Oliver 1979). For all experiments, a reference sample (usually metallic Fe) was used to provide an internal and accurate energy calibration of the monochromator for all spectra (first inflection point of the Fe *K*-edge set at 7111.08 eV). The reproducibility of the monochromator energy was defined by a Heidenhain goniometer angle encoder within a tolerance of $2 \cdot 10^{-5}$ degree.

An additional set of spectra recorded at lower spectral resolution was collected at BESSY (Berlin, Germany) on the bending-magnet beamline KMC-2. The storage ring conditions were 1.7 GeV and 120–240 mA electron current. An Si-Ge (111) gradient two-crystal monochromator was used, providing an energy resolution $E/\Delta E = 4000$ (Erko et al. 2000).

All spectra were collected in fluorescence mode using a Stern-Heald type detector (Lytle et al. 1984), which was filled with krypton. Ionization chambers were used for measuring the beam intensity before and after passing the sample (filled with N_2 and Ar, respectively). XANES spectra were collected from ~60 eV below to 200 eV above the Fe *K*-edge (7050–7300 eV), with 0.1 eV steps for the pre-edge region (7108–7116 eV). The XANES spectra were background corrected by fitting the spectral region from 7050 to 7090 eV (the region before the pre-edge) using a polynomial and subtracting it as background absorption. The spectra were then normalized for atomic absorption, based on the average absorption coefficient of the spectral region from 7200 to 7300 eV (i.e., after the edge crest). The pre-edge of the spectra taken on glass and melt was modeled by fitting two Gaussian functions for the pre-edge peaks and two further Gaussian functions to model the contribution of the main-edge to the pre-edge background using a part of the spectra between 7104 and 7118 eV (see Wilke et al. 2004 for further details). The pre-edge of the spectra taken on the crystalline reference materials was modeled in a slightly different way by fitting two pseudo-Voigt functions for the pre-edge peaks. This is due to differences in the pre-edge peak shape between amorphous and crystalline compounds (Wilke et al. 2004, 2001). The pre-edge background was modeled in the same way as for the glasses and melt. Only high-resolution spectra were used for the pre-edge analysis. The pre-edge information was derived by calculating the total integrated area and the centroid (area-weighted average of the pre-edge peak position) of the fitted pre-edge feature.

For the high-temperature in-situ measurements, pieces of the starting glasses were heated using a $Pt_{70}Rh_{30}$ wire-loop furnace as described by Farges et al. (1996). The temperature was controlled using an S-type thermocouple that was in contact with the melt. The uncertainty of the temperature is estimated to be about ±15 K due to a possible temperature gradient across the sample between PtRh-loop and thermocouple. During the experimental runs, the temperature was constant within ±2 K. The heating loop was held in a sealed aluminum case, which was flushed with gas to control the furnace atmosphere. Experiments at reducing conditions were controlled by flushing the furnace with nitrogen that contained 4% hydrogen. Experiments at oxidizing conditions were performed in air. After the run, samples were quenched simply by switching off the power. The samples cooled down below 300 °C within one minute. The furnace apertures for both the incoming monochromatic beam and outgoing fluorescence radiation were covered by a 14 µm thick Mylar foil. In addition, the fluorescence detector was protected by an 8 µm thick aluminized Tennolan foil, which reduced the heat load on the detector from the black-body radiation.

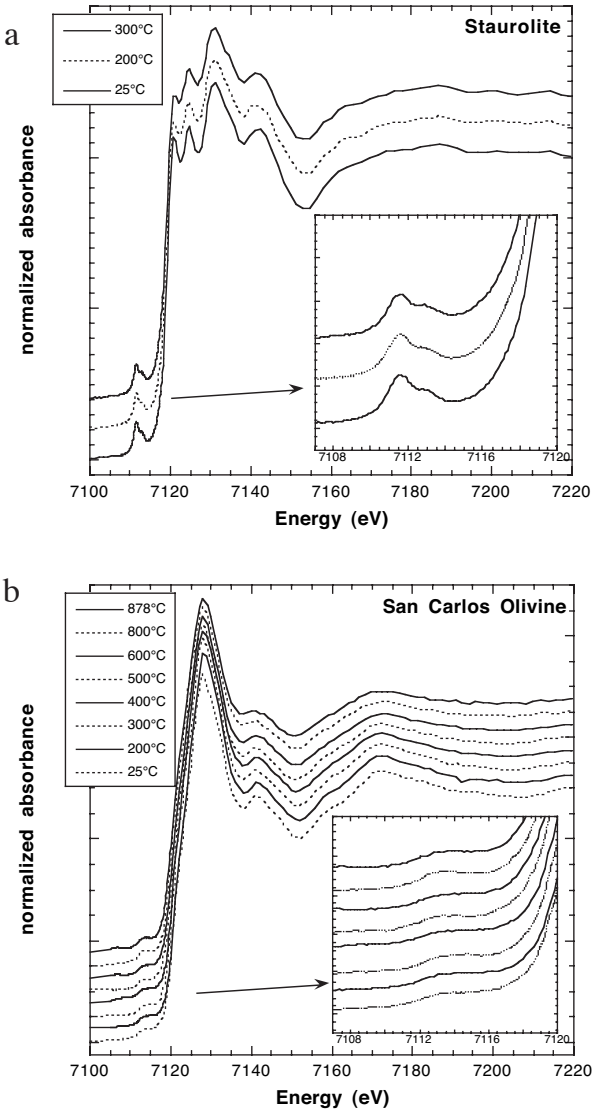

FIGURE 1. (**a**) Normalized Fe *K*-edge XANES spectra of staurolite measured with high spectral resolution at the temperatures indicated. The inset shows a zoom of the pre-edge region. (**b**) Normalized Fe *K*-edge XANES spectra of olivine measured with low spectral resolution at the temperatures indicated. The inset shows a zoom of the pre-edge region.

RESULTS AND DISCUSSION

XANES of two model compounds are shown in Figure 1. These are used for an improved evaluation of the spectra of glasses and melt. XANES of the samples collected on the glass at room temperature and on the melt at high temperature are shown in Figure 2 (oxidized conditions) and Figure 3 (reduced conditions). Figure 4 displays the corresponding pre-edge features modeled from the fitted Gaussians. Figure 5 shows the pre-edge information (integrated intensity and the centroid position, according to Wilke et al. 2001) that was derived from the pre-edge fits.

The pre-edge centroid position provides an estimate of the Fe-oxidation state in the sample, as shown by Wilke et al. (2004) and Berry et al. (2003) who used correlations of pre-edge data with Mössbauer spectroscopic data. Based on the calibration given by Wilke et al. (2004), the $Fe^{3+}/\Sigma Fe$ ratio of the samples measured under reducing conditions was below 0.08 (unless noted otherwise). The $Fe^{3+}/\Sigma Fe$ ratio of the samples measured at oxidizing conditions was above 0.8. The changes in the speciation of Fe between glass and melt were analyzed by investigation of both the pre-edge feature and the position of the first maximum of the EXAFS oscillation. We point out that the combination of both features is required to derive reliable speciation information for Fe in such systems. An increase in

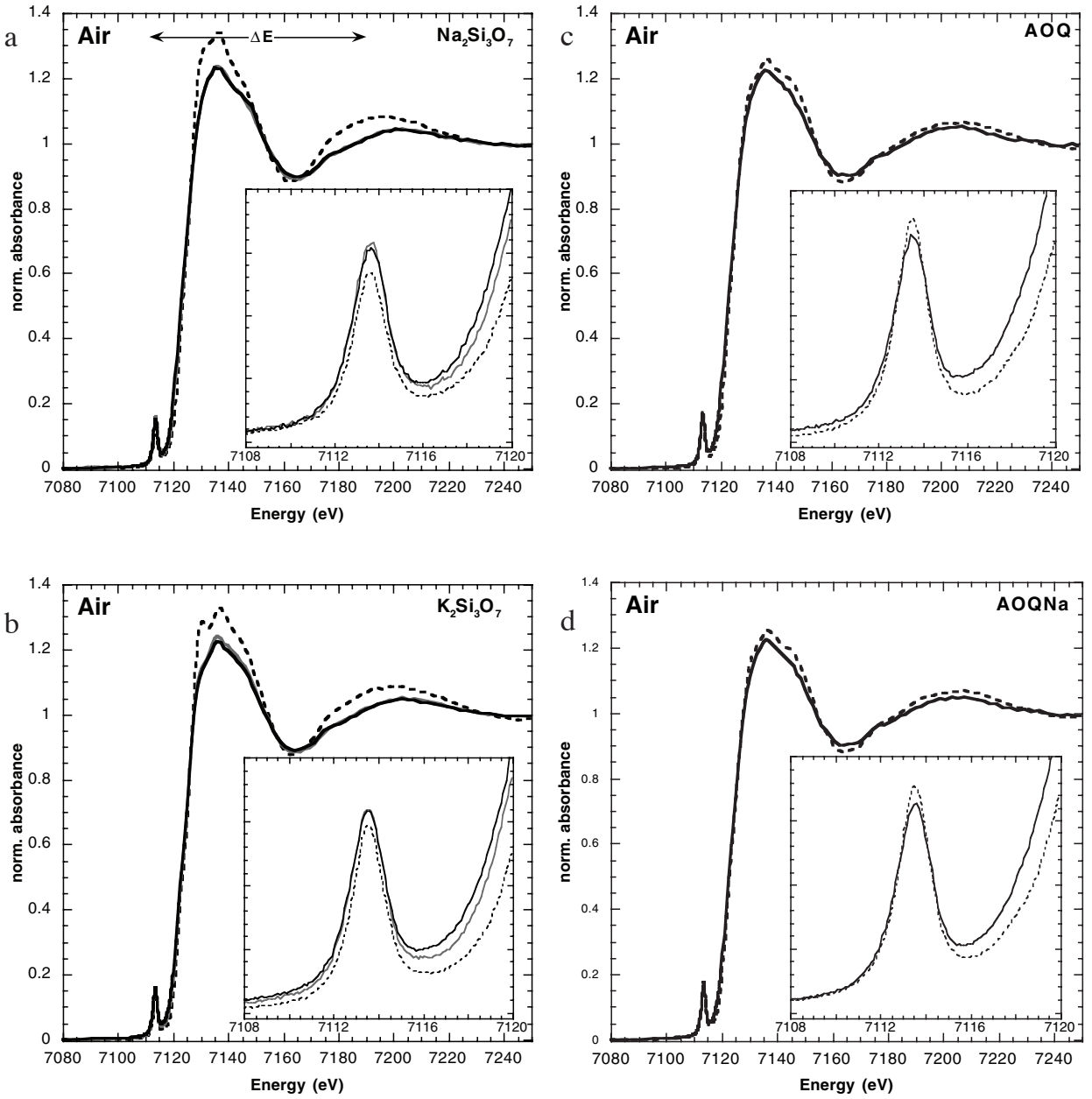

FIGURE 2. Normalized Fe *K*-edge XANES spectra of oxidized samples of compositions indicated, collected at both high and room temperatures. The insets show a zoom of the pre-edge region: (**a**) $Na_2Si_3O_7$, dashed line = glass after run; gray solid line = melt at 850 °C; dark solid line = melt at 950 °C. (**b**) $K_2Si_3O_7$, dashed line = glass after run; gray solid line = melt at 850 °C; dark solid line = melt at 950 °C. (**c**) AOQ, dashed line = glass after run; dark solid line = melt at 1050 °C. (**d**) AOQNa, dashed line = glass after run; dark solid line = melt at 1050 °C.

the pre-edge intensity can be related to changes in the symmetry of the coordination environment (e.g., Waychunas et al. 1983; Westre et al. 1997; Wilke et al. 2001). Strictly speaking, an increase in the pre-edge intensity indicates a loss of centrosymmetry, which could result, e.g., from a change from octahedral to tetrahedral geometry, as shown in the variogram in Figure 5. Distortions of the octahedral geometry also yield higher pre-edge intensities, but to a much smaller extent (cf. Wilke et al. 2001). Therefore, another constraint in the spectra is required to distinguish between distortion and coordination changes. For this, the position of the first EXAFS maximum is particularly useful because it is inversely related to the Fe-O distance, which depends directly on the number of first neighbors around the central Fe. Thus, quite reliable information on the speciation of Fe (oxidation state and coordination) can be obtained from the symmetry and the average Fe-O distance.

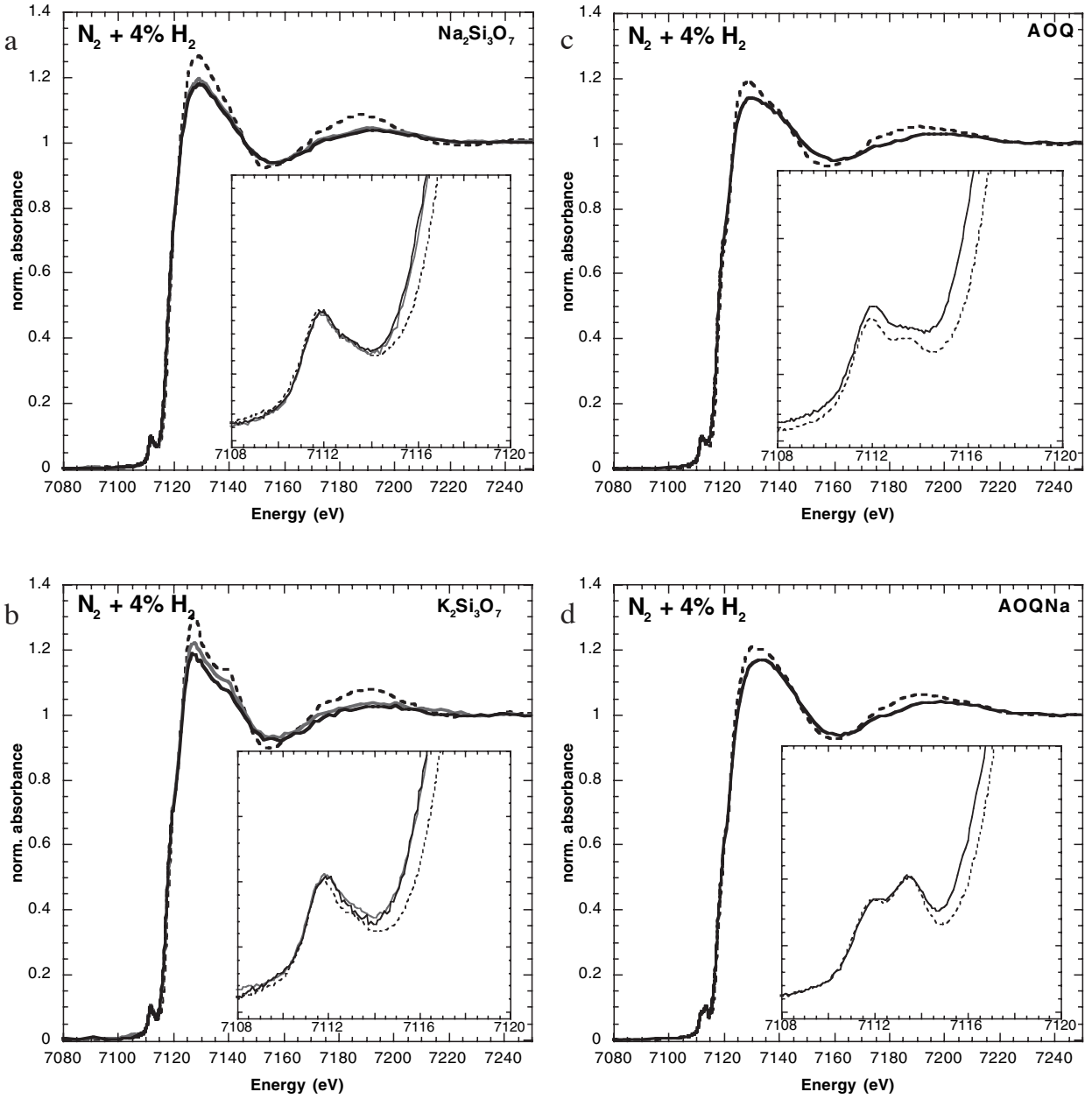

FIGURE 3. Normalized Fe *K*-edge XANES spectra of reduced samples of compositions indicated, collected at high and room temperatures. The insets show a zoom of the pre-edge region: (**a**) $Na_2Si_3O_7$, dashed line = glass after run; gray solid line = melt at 850 °C; dark solid line = melt at 950 °C. (**b**) $K_2Si_3O_7$, dashed line = glass after run; gray solid line = melt at 850 °C; dark solid line = melt at 950 °C. (**c**) AOQ, dashed line = glass after run; dark solid line = melt at 1050 °C. (**d**) AOQNa, dashed line = glass after run; dark solid line = melt at 1050 °C.

Model compounds

Temperature-dependent measurements of model compounds were made to estimate the potential influence of temperature-induced anharmonicity on the spectra. The effect of anharmonicity is assumed to be small in the energy region close to the edge (Brown et al. 1995). We only investigated the temperature dependence of ferrous compounds, for which anharmonic effects are expected to be largest (Farges and Brown 1996). Figures 1a and 1b show XANES spectra of staurolite and olivine as a function of temperature. An analysis of the pre-edge of the high-resolution staurolite spectra revealed only minor changes in the pre-edge between room temperature and 300 °C, as shown by the pre-edge parameters plotted in Figure 5. At higher temperatures, staurolite decomposed, and no further investigation was possible. Although the temperature range was limited, these data indicate that the temperature effect on the pre-edge for constant site geometry is probably only of minor importance. Furthermore, the position of the first EXAFS maximum also was not affected in this temperature interval. Spectra of olivine were acquired up to 880 °C. However, the low resolution of these spectra did not

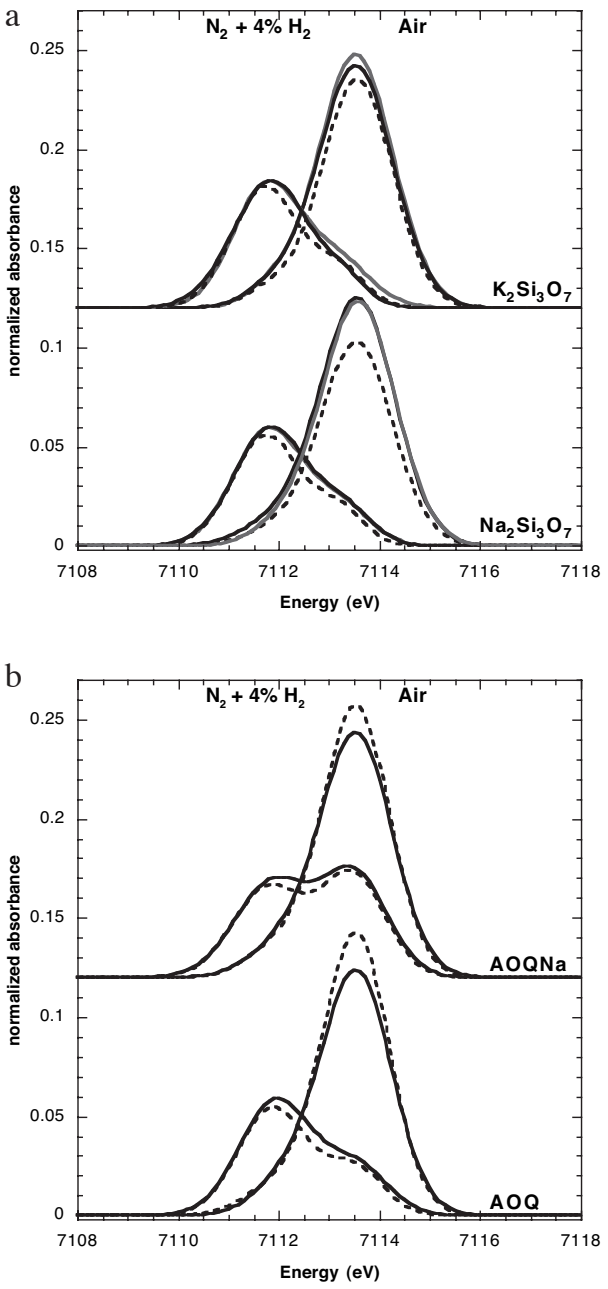

FIGURE 4. (**a**) Fitted pre-edges of oxidized and reduced alkali-silicate compositions as indicated. (**b**) Fitted pre-edges of oxidized and reduced haplogranitic compositions as indicated. (For explanation of symbols, see Figs. 2 and 3 captions).

permit detailed pre-edge analysis. Qualitative inspection of the pre-edge does not reveal major changes in the pre-edge region (Fig. 1b). In addition, in the EXAFS region (which is less sensitive to the spectral resolution), the amplitude of the EXAFS oscillation decreases with temperature, which can be attributed to thermal disorder. No significant shift in the position of the first EXAFS maximum was observed, which indicates that the effect of anharmonicity in this region of the spectrum is quite small (see below for a more detailed analysis).

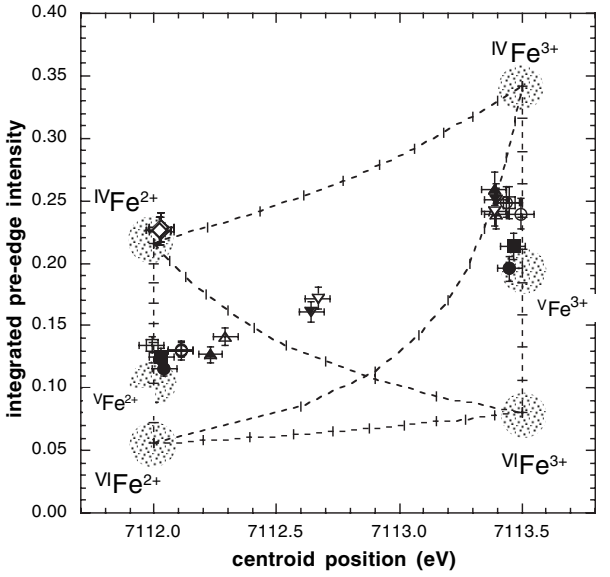

FIGURE 5. Pre-edge parameters of all samples plotted in the variogram after Wilke et al. (2001). Gray fields designate pre-edge parameters for the Fe coordination and oxidation state indicated. Dashed lines between fields indicate the variation of pre-edge parameters assuming binary mixtures of respective end-members. Ticks on curves refer to the percentage of mixtures. Solid symbols = samples at room temperature; open symbols = samples at high temperature. Circles = $Na_2Si_3O_7$; squares = $K_2Si_3O_7$; triangles = AOQ; inverted triangles = AOQNa; diamonds = staurolite.

Oxidized alkali-silicate compositions

The spectra of both compositions, $K_2Si_3O_7$ (KS3) and $Na_2Si_3O_7$ (NS3), show significant differences between the glass and the melt (Figs. 2a and 2b). The intensity of the pre-edge of the melt is higher, the fine structure at the main crest of the edge changes, and the position of the first maximum of the EXAFS is shifted toward higher energies. The higher pre-edge intensity observed for the high-temperature melt indicates a higher amount of sites with no centrosymmetry. As the average coordination geometry is likely to be an average of a mixture of tetrahedral, octahedral, and trigonal-bipyramidal geometries, as was encountered previously for Fe in glasses and melts (Brown et al. 1995; Farges et al. 2004; Jackson et al. 2005), the increased pre-edge intensity suggests an increased number of tetrahedrally coordinated Fe compared to the quenched glass. This finding also is consistent with the shift of the first EXAFS maximum to higher energies, which indicates a decrease in the mean Fe-O distance. The pre-edge intensity of the glassy samples indicates an average Fe^{3+} coordination number of about 5 assuming that the coordination polyhedra mentioned above are present, whereas the spectra of the molten samples indicate an average coordination of 4.6 to 4.7 (see Fig. 5).

Oxidized haplogranitic compositions

The Fe *K*-edge XANES spectra for the haplogranitic composition (AOQ) also display differences between the glass and the melt (Fig. 2c), although these differences are much smaller. In this case, however, the pre-edge intensity is slightly lower

in the molten state, the fine structure at the main crest does not change, and the first maximum of the EXAFS does not shift. These observations indicate that the local structure around Fe in glass and melt was similar and only slight symmetry changes occurred (i.e., fewer sites without centrosymmetry).

The XANES spectra of the peralkaline haplogranitic composition (AOQNa) show almost the same differences between the glass and the melt as described for the metaluminous haplogranitic composition (Fig. 2d). In addition, the metaluminous and the peralkaline compositions display very similar pre-edge intensities. Apparently, the degree of peralkalinity has no major effect on the local structure around Fe, although the addition of Na_2O affects the polymerization of the melt network as indicated, for example, by the strong decrease in the melt viscosity as a function of the Na content (e.g., Hess et al. 1995) and by spectroscopic observations (e.g., Mysen 1988).

Reduced alkali-silicate compositions

The XANES spectra of reduced KS3 and NS3 show small differences between glass and melt (Figs. 3a and 3b). The intensity of the pre-edge feature is slightly higher in the melt, the fine structure at the main crest changes significantly only for KS3, and the position of the first EXAFS maximum is shifted slightly toward higher energies for the molten state. The differences between the glassy and the molten states may be interpreted in a manner similar to those of the oxidized samples. Thus, a slightly higher amount of low-coordinated Fe was found in the reduced melts at high temperature. The observed changes in the pre-edge between melt and glass are much smaller than reported by Jackson et al. (1993) for molten fayalite. As stated above, this difference is probably related to the normalization procedure. Normalization of the spectra to the XANES maximum results in an artificial increase of the pre-edge intensity of high-temperature spectra. This is due to a decrease of the XANES maximum by thermal disorder in the melt, as observed for Ni and Ti (Farges et al. 1996; Farges et al. 1994). The purpose of normalization is to account for differences in the element concentration, which is directly related to the height of the edge jump. Intensities of spectral resonances (such as the maximum of the XANES or any amplitude in the EXAFS oscillations) are features related to the melt structure around Fe, which should not be used for normalization.

Reduced haplogranitic compositions

The XANES spectra of the reduced haplogranitic composition (Fig. 3c) show differences between the melt and the glass that are similar to those observed for the reduced alkali-silicate compositions. The pre-edge intensity is slightly higher in the melt, the fine structure at the main crest does not change in this case, and the first EXAFS maximum is shifted slightly toward higher energies. Thus, the spectra indicate a slight increase of low-coordinated Fe in the reduced haplogranitic melt. The shift in the centroid position of haplogranite compared to that of NS3 and KS3 reflects a higher content of Fe^{3+}, which is probably related to the difference in the melt composition.

The spectra of the peralkaline haplogranitic composition show an even larger shift of the pre-edge centroid position toward higher energies for both the glass and the melt (Fig. 3d), which indicates a significantly higher amount of Fe^{3+} compared to the metaluminous haplogranitic composition. This was observed consistently in several independent experimental runs and, therefore, cannot be related to changes in the redox conditions of the setup, e.g., by leakage of the cell. Thus, the addition of excess Na_2O promotes a higher amount of Fe^{3+} for the same redox conditions consistent with previous findings (Mysen et al. 1985; Mysen 1988). In addition to this feature, the peralkaline composition showed differences between the melt and the glass similar to those described for the reduced metaluminous haplogranitic composition and, thus, a slightly higher amount of low-coordinated Fe moieties in the melt compared to its quenched glass.

Pre-edge feature vs. estimates of Fe-O distance

As mentioned above, the coordination of Fe is correlated directly to the Fe-O distance. Natoli (1983), Bianconi et al. (1983), and Wu et al. (1997, 1999) showed that the position of the first maximum of the EXAFS can be related to the average distance, R, between absorbing element and the first coordination shell using the equation:

$$\Delta E \times R^2 = \text{constant} \quad (1)$$

where ΔE is the difference in energy between the first EXAFS maximum and the onset of the edge. The maximum of the pre-edge feature was taken as reference point for the edge onset (see also Fig. 2). The value of the constant depends mainly on the absorbing and backscattering elements. Because ΔE is a sensitive marker for changes in the Fe-O distance, a correlation between ΔE and the pre-edge intensity can be used to support the pre-edge based observations and interpretations. Figure 6 shows that the pre-edge intensity is well correlated to ΔE for both the reduced and the oxidized samples. This correlation strongly indicates that the pre-edge can be used as a quite sensitive tool to detect changes in the coordination polyhedron, at least in the specific case of Fe in oxide glasses and melts.

Assuming that the constant in Equation 1 is independent of temperature, the measured ΔE values provide an estimate of the ratio of the Fe-O distance between the glass (R_{RT}) and the melt at high temperature (R_{HT}) using the equation

$$\Delta E_{RT} \times R_{RT}^2 = \Delta E_{HT} \times R_{HT}^2 \quad (2)$$

which can be rearranged to

$$(E_{RT}/\Delta E_{HT})^{0.5} = R_{HT} / R_{RT}. \quad (3)$$

For glasses and melts, this method yields reliable average Fe-O distances, because the medium-range environment does not interfere significantly with the EXAFS signal for the Fe-O pair (Bugaev et al. 2005). For model compounds and melt samples, the R_{HT}/R_{RT} ratios determined in this study are plotted in Figure 7 vs. the temperature difference of the measurements. The ratios derived from the set of data acquired with lower spectral resolution also are included. The determined ratios are similar to those from the high-resolution scans as shown in Table 2. This is because EXAFS is less sensitive to the spectral resolu-

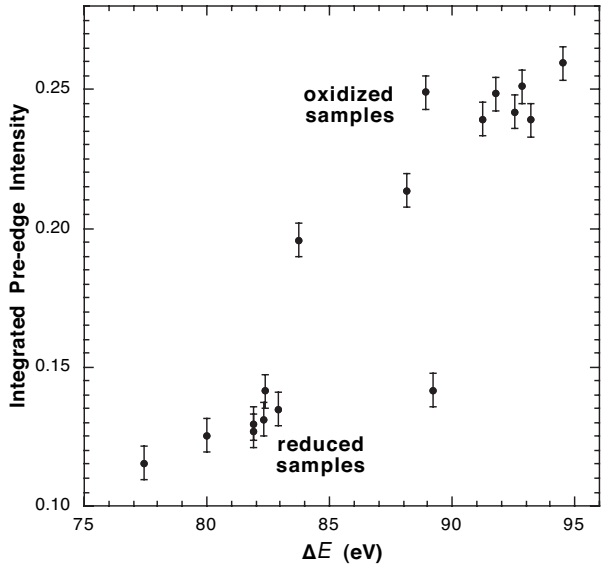

FIGURE 6. Plot of pre-edge intensity vs. position of the first EXAFS-maximum. D*E* denotes the energy difference between first EXAFS maximum and the maximum of the pre-edge. The graph shows a good correlation between the two parameters, indicating that the observed changes in the spectra are related to changes in the structural environment of Fe in the samples.

tion than XANES or the pre-edge region. The error bars shown in Figure 7 are based on an estimated uncertainty of ±0.2 eV in the determination of Δ*E* from the spectra. The experimentally determined ratios are compared to various predictions, which were computed for a given coordination polyhedron using the compilation of Brown et al. (1995) and linear thermal expansion coefficients from Hazen and Finger (1982). The calculated trends show that the expected increase in the Fe-O distance with temperature is quite small for the considered temperature interval. The maximum increase is less than 1% for Fe^{3+} and less than 2% for Fe^{2+}, depending on coordination. The samples should plot along these lines if no change in Fe coordination occurs. A decrease in the coordination number of Fe would result in a smaller Fe-O distance and, thus, a decrease in the ratio, as shown by the dashed lines for a change from C_{3h} (trigonal bipyramid) to T_d (tetrahedral) symmetry.

Model compounds

The high-temperature olivine spectra were analyzed to estimate the effect of anharmonicity on the position of the first EXAFS maximum. In the case of crystalline compounds, contributions from next-nearest neighbors to the EXAFS signal influence the position of the first EXAFS maximum (Bugaev et al. 2005). Thus, the position of the maximum determined from the spectra of olivine is certainly not correct for the corresponding Fe-O distance and is not transferable to other compounds. However, a relative comparison of the spectra collected on olivine at different temperatures is still feasible. If anharmonicity affects the position of the first EXAFS maximum, the resulting R_{HT}/R_{RT} ratios will be smaller than the expected values (Brown et al. 1995). The data plotted in Figure 7 indicate that, above a temperature difference of 300 K, the R_{HT}/R_{RT} determined from the spectra underestimates the expected values by up to approximately 2% at 800 to 880 °C. Fe^{2+} in olivine is in distorted octahedral coordination and thus has a significantly higher coordination than the average coordination of about five reported for Fe^{2+} in glasses (e.g., Rossano et al. 2000). The XAFS spectra of lower coordinated cations are affected to a lesser extent, because the strength of anharmonicity is related inversely to the bond valence of a given bond (Farges and Brown 1996; Brown et al. 1995; bond valence of $^{VI}Fe^{2+}$: 0.33 v.u., bond valence of $^{IV}Fe^{2+}$: 0.5 v.u., see also below).

Grandidierite, $(Mg,Fe)Al_3BsiO_9$, can be used as a model compound for fivefold-coordinated Fe^{2+} (Farges 2001; Seifert and Olesch 1977). Inspection of high-temperature spectra of this compound could provide a better estimate of anharmonicity for the average coordination found in glass and melt. However, the acquisition of high-temperature spectra in the temperature range of interest is not possible due to decomposition of the compound. Therefore, simulated spectra of grandidierite were used to provide at least a rough estimate of the effect of anharmonicity. The XAFS spectra can be simulated quite confidently using the feff code (vers. 8.2, Ankudinov et al. 1998) if the compounds are not too complex chemically, as shown by e.g., Farges (2001) and Farges et al. (1997). The contribution of anharmonicity to the simulated spectra from thermally induced disorder is based on the correlated Debye model. The spectra at room temperature and 1300 °C were simulated only for the FeO_5 coordination polyhedron, which occurs in the crystal structure of grandidierite, based on the structure refinement by Stephenson and Moore (1968). The restriction of the simulation to the first oxygen shell avoids the superposition of the EXAFS signal by more distant shells around Fe (for more details on the simulation see Farges 2001). The position of the first EXAFS maximum of the simulated spectra was determined using the same procedure as for the measured spectra. The R_{HT}/R_{RT} ratio determined for a temperature difference of 1275 K deviates from the value expected from the thermal expansion by about 1%. That is, the deviation is significantly smaller than the one determined from the experimental data for Fe^{2+} in olivine. Therefore, we conclude that the R_{HT}/R_{RT} ratio for the glasses and melts is probably underestimated by about 1% if the proposed analytical procedure performed on the experimental data is utilized.

Glass/melt samples

All reduced samples showed a significant decrease in the R_{HT}/R_{RT} ratio, which was larger than the one measured on olivine. The decrease found for olivine is probably related to anharmonicity. As explained above, the effect of anharmonicity is expected to be smaller for Fe in glass and melt due to a lower average coordination. If a systematic underestimation of about 1% is assumed, the observed decrease in the R_{HT}/R_{RT} ratio still indicates a decrease in the average coordination number of Fe, which was already inferred indirectly from the pre-edge intensity changes. The observed change in the Fe-O distance of the reduced alkali silicates is considerably smaller than the one calculated for a change from C_{3h} to T_d symmetry, particularly if the underestimation due to anharmonicity is considered.

For the reduced haplogranite, the observed uncorrected

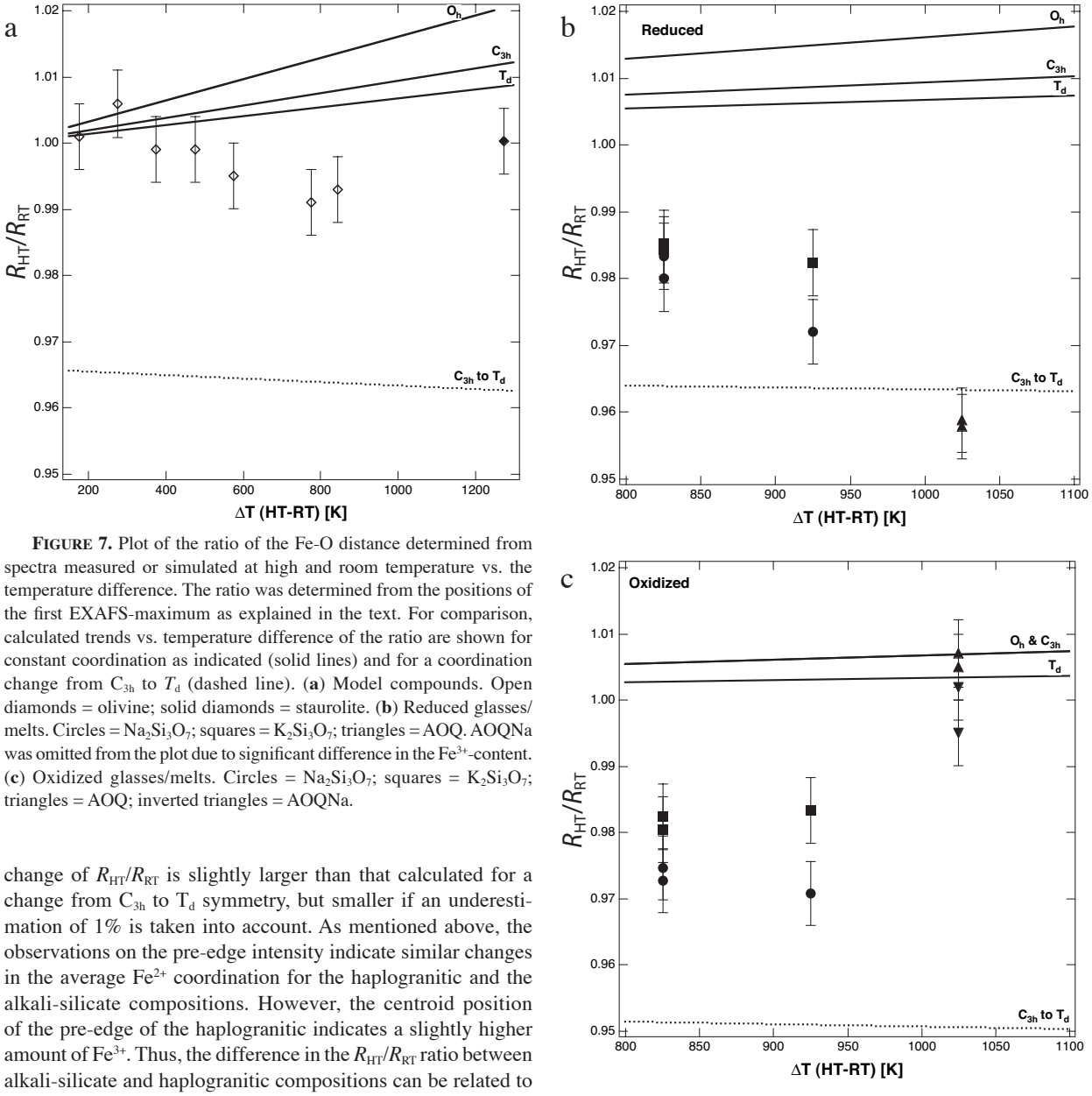

FIGURE 7. Plot of the ratio of the Fe-O distance determined from spectra measured or simulated at high and room temperature vs. the temperature difference. The ratio was determined from the positions of the first EXAFS-maximum as explained in the text. For comparison, calculated trends vs. temperature difference of the ratio are shown for constant coordination as indicated (solid lines) and for a coordination change from C_{3h} to T_d (dashed line). (**a**) Model compounds. Open diamonds = olivine; solid diamonds = staurolite. (**b**) Reduced glasses/melts. Circles = $Na_2Si_3O_7$; squares = $K_2Si_3O_7$; triangles = AOQ. AOQNa was omitted from the plot due to significant difference in the Fe^{3+}-content. (**c**) Oxidized glasses/melts. Circles = $Na_2Si_3O_7$; squares = $K_2Si_3O_7$; triangles = AOQ; inverted triangles = AOQNa.

change of R_{HT}/R_{RT} is slightly larger than that calculated for a change from C_{3h} to T_d symmetry, but smaller if an underestimation of 1% is taken into account. As mentioned above, the observations on the pre-edge intensity indicate similar changes in the average Fe^{2+} coordination for the haplogranitic and the alkali-silicate compositions. However, the centroid position of the pre-edge of the haplogranitic indicates a slightly higher amount of Fe^{3+}. Thus, the difference in the R_{HT}/R_{RT} ratio between alkali-silicate and haplogranitic compositions can be related to this difference in the Fe^{3+} content, because the mean Fe-O distance depends also strongly on the oxidation state and thus also affects the position of the first EXAFS maximum.

The R_{HT}/R_{RT} ratios of the oxidized alkali-silicate compositions indicate a similar behavior compared to their reduced counterparts, i.e., a decrease in the average Fe coordination number. The decrease is smaller than the one calculated for a change from C_{3h} to T_d symmetry. In the case of Fe^{3+}, the contributions from anharmonicity are expected to be smaller than for Fe^{2+} due to the higher charge and, thus, the higher bond valence (Farges and Brown 1996). Therefore, no correction was applied. The R_{HT}/R_{RT} ratios of the oxidized metaluminous haplogranitic and peralkaline haplogranitic samples are consistent with the calculated trends at constant average Fe coordination, indicating no or little change in the average Fe coordination number.

Structural changes around Fe at T_g—relationship to melt network?

The difference between the glassy and the molten states (with respect to the Fe coordination polyhedron) potentially may be explained as a response to structural changes in the bulk melt network. A systematic variation in the pre-edge intensity with the type of the major network modifier present in the glass (Na, K, Mg) was observed in a study on Fe in Ca-bearing silicate glasses (Farges et al. 2004). This implies that the Fe coordination varies with the average bond valence of these cations. High pre-edge intensities are observed for small bond valences (K-bearing) and low intensities for high bond valences (Na, Mg). Thus, a network modifier with a low bond valence will favor low-coordinated Fe. Such a relation also was found for Ni^{2+} in silicate glass, where the

TABLE 2. Fe pre-edge intensity and centroid position determined from high-resolution XANES spectra

	Integrated intensity ±5% rel.	Centroid pos. (eV) ±0.05	R_{HT}/R_{RT} high resol.	R_{HT}/R_{RT} low resol.	ΔE (eV) high resol.	ΔE (eV) low resol.	Av. bond valence of cations (v.u.)*
NS3 ox. RT	0.1957	7113.53	n.a.	n.a.	83.76	83.12	0.210
NS3 ox. 850 °C	0.2396	7113.50	0.973	0.975	88.53	87.44	0.184
NS3 ox. 950 °C	0.2490	7113.52	0.971	n.d.	88.91	n.d.	0.181
NS3 red. RT	0.1154	7112.04	n.a.	n.a.	77.40	77.07	0.210
NS3 red. 850 °C	0.1295	7112.11	0.980	0.984	80.64	79.62	0.184
NS3 red. 950 °C	0.1312	7112.11	0.972	n.d.	81.92	n.d.	0.181
KS3 ox. RT	0.2136	7113.46	n.a.	n.a.	88.17	87.13	0.140
KS3 ox. 850 °C	0.2483	7113.45	0.980	0.982	91.77	90.31	0.110
KS3 ox. 950 °C	0.2394	7113.44	0.983	n.d.	91.25	n.d.	0.108
KS3 red. RT	0.1253	7112.03			79.99	78.76	0.140
KS3 red. 850 °C	0.1413	7112.15	0.985	0.983	82.39	81.41	0.110
KS3 red. 950 °C	0.1347	7111.99	0.982	n.d.	82.94	n.d.	0.108
AOQ ox. RT	0.2595	7113.39	n.a.	n.a.	94.51	92.90	0.175
AOQ ox. 1050 °C	0.2391	7113.40	1.007	1.005	93.21	92.06	0.142
AOQ red. RT	0.1270	7112.23	n.a.	n.a.	81.90	78.71	0.175
AOQ red. 1050	0.1416	7112.29	0.958	0.959	89.22	85.69	0.142
AOQNa ox. RT	0.2511	7113.40	n.a.	n.a.	92.87	91.47	n.d.
AOQNa ox. 1050 °C	0.2419	7113.39	1.002	0.995	92.56	92.46	n.d.
AOQNa red. RT	0.1608	7112.64	n.a.	n.a.	81.00	79.13	n.d.
AOQNa red. 1050 °C	0.1719	7112.67	0.966	0.962	86.85	85.39	n.d.

Notes: The ratio (R_{HT}/R_{RT}) of the Fe-O distance between glass and melt was determined from the position (ΔE) of the first EXAFS-maximum. Results from low-resolution XANES spectra are also reported. n.d. = not determined; n.a. = not applicable.
* v.u. = valence units.

pre-edge intensity increases with decreasing bond valence of the network-modifying cation, i.e., from Ca via Na to K (Farges et al. 2001). This behavior is a direct consequence of Pauling's second rule, which states that the sum of the bond valences of a given ion should equal the formal charge. To keep the bond-valence sum of O atoms surrounding Fe at the nominal value of 2, Fe has to be fourfold-coordinated in K-silicate compositions (bond valence of K: 0.12) and fivefold-coordinated in Na-silicate compositions (bond valence of Na: 0.16) (cf. Farges et al. 2004).

In a similar manner, an increase in temperature decreases the average bond valence of a given network modifier (e.g., Na, K) due to the increase of the cation-oxygen distance related to thermal expansion. In an extreme case, this temperature-induced change in the bond valence potentially can affect the Fe coordination in the same way, i.e., a similar effect as replacing Na by K. For a given temperature, the average bond valence s for a cation can be calculated using the relationship of Brown and Altermatt (1985).

$$s = \exp[(R_0 - R)/0.37]. \quad (4)$$

The mean cation-oxygen distance R for a given temperature was calculated using the compilation of ionic radii of cations for coordination numbers given by Brown et al. (1995) and the linear thermal expansion coefficient given by Hazen and Finger (1982). R_0 is the bond-valence parameter taken from Brese and O'Keeffe (1991), which is dependent on the cation and its valence state. The bond-valence values were calculated for the respective network-modifying cation (Na or K) in the case of the alkali silicates. For the metaluminous haplogranite, the effective bond valence was based on the relative abundance of Na and K. The relationship between the pre-edge intensity and the calculated average bond valence of the alkali cation at a given temperature is shown in Figure 8a.

At reducing conditions, the *alkali-silicate compositions* show a slight increase of the pre-edge intensity with decreasing bond valence, i.e., increasing temperature. The data for both K and Na apparently plot on a common trend, which may simply be a result of the small differences observed in the pre-edge intensities. At oxidizing conditions, an increase of the pre-edge intensity with decreasing bond valence also was observed for the alkali-silicate compositions. As the temperature-induced change is much larger, the data for oxidized NS3 and KS3 do not plot on a common trend. If only room-temperature data are considered, the trend of the data still is consistent with the relationship between the type of network modifier and Fe coordination (and thus pre-edge intensity) observed by Farges et al. (2004). The relative change of the pre-edge intensity with temperature is shown in Figure 8b, where pre-edge intensities measured for high-temperature samples were normalized to the values measured at room temperature. Plotted in such a way, the pre-edge intensity changes between glass and melt are similar within error for all alkali-silicate samples except for the oxidized NS3, which shows a stronger increase than the other samples. The pre-edge intensity of the reduced *haplogranitic composition* is located on the apparent trend defined by the reduced alkali-silicate compositions in Figure 8a. Furthermore, the relative change is also similar to those found for the reduced alkali silicates. In contrast, the *oxidized haplogranitic composition* showed a slight decrease of the pre-edge intensity with increasing temperature (Figs. 8a and 8b). Therefore, these samples plot far away from the trend of the other samples.

No clear relationship between the temperature-induced changes in the average bond valence of the alkali cations and the pre-edge intensity can be deduced from this plot. This may imply that structural changes in the bulk melt only play a minor role for the observed differences of the local environment of Fe between glass and melt. In light of these considerations, the observed differences between glass and melt appear to be induced by local adaptation of the Fe-O polyhedron to the melt structure. Still, the strong changes observed for the oxidized alkali-silicate samples are rather unexpected because the potential for differ-

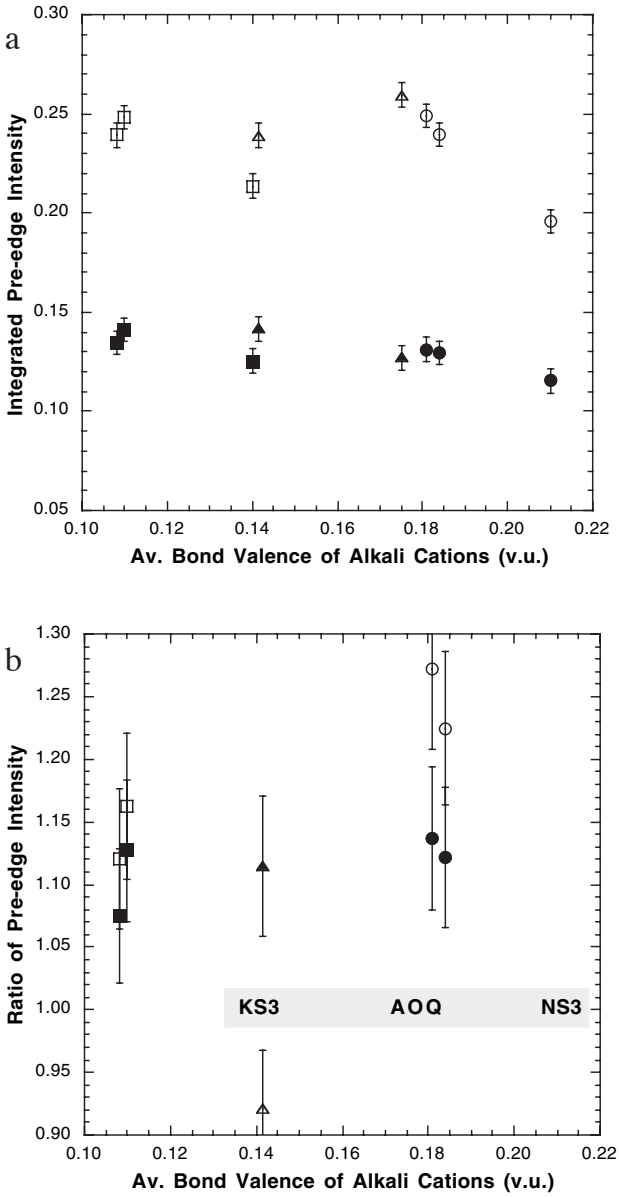

FIGURE 8. (**a**) Plot of the pre-edge intensity vs. the calculated average bond valence of the alkali cations. Lower values of the bond valence for a given composition refer to higher temperatures (see also Table 2 and text). Solid Circles = reduced $Na_2Si_3O_7$; solid squares = reduced $K_2Si_3O_7$; solid triangles = reduced AOQ; open circles = oxidized $Na_2Si_3O_7$; open squares = oxidized $K_2Si_3O_7$; open triangles = oxidized AOQ. (**b**) Plot of relative changes of the pre-edge intensity vs. calculated bond valence. Pre-edge intensities were normalized to the values obtained at room temperature. Annotations in the shaded area indicate bond valence values at room temperature.

ences in the local structural environment between glass and melt is expected to be smaller for higher charged cations (Farges and Brown 1996).

Implications and concluding remarks

A comparison of the XANES spectra taken on glass at room temperature and on melt at high temperature provides some evidence that there are differences between glass and melt in the local structural environment of Fe. In case of reduced samples, the pre-edge intensities in the glass and its melt are both consistent with mixtures of fivefold- and fourfold-coordinated Fe^{2+} for all compositions, as suggested previously (e.g., Brown et al. 1995; Rossano et al. 2000; Galoisy et al. 2001). In spectra collected on the melt, both the pre-edge and the position of the first EXAFS-maximum indicate a slight increase in the amount of tetrahedrally coordinated Fe^{2+} compared to the glass. However, the change of the pre-edge intensity indicates that the concentration of tetrahedrally coordinated Fe^{2+} increases by at most 10% (Fig. 5), and the shift in the position of the first EXAFS maximum is consistent with this estimate. This finding contrasts with previous studies (Waychunas et al. 1988; Jackson et al. 1993) in which a complete conversion of higher-coordinated (e.g,. sixfold- and fivefold-coordinated) to fourfold-coordinated Fe^{2+} in the melt was suggested. The change in the pre-edge of Fe^{2+}-dominated samples appears to be similar for alkali-silicate and haplogranitic compositions, despite the difference in melt polymerization. However, the two compositions may not be directly comparable due to the higher amount of Fe^{3+} in the haplogranitic sample.

A more complex picture is derived from the data of the oxidized samples. The pre-edge intensities indicate that a mixture of coordination environments also exists for Fe^{3+}. For the molten state, an increase of tetrahedrally coordinated Fe^{3+} of about 10–20% was only found for the alkali-silicate compositions. In the case of the haplogranitic samples, the spectra indicate only minor changes in the average Fe coordination above T_g. Thus, the influence of the bulk composition on the temperature-dependent behavior of Fe^{3+} appears to be much larger. One possible explanation for the distinct temperature-dependent behavior is the difference in the polymerization of the melts, which is related directly to the transport properties such as viscosity or diffusivity (e.g., Chakraborty 1995). Due to the higher mobility of elements in the more depolymerized compositions, the structural changes are stronger during cooling through the temperature region of the supercooled liquid and T_g. Such changes may substantially influence the local structure around Fe during the quench. This relationship suggests that any parameter which increases the amount of NBO in the glass/melt system, such as water and fluorine content or peralkalinity, should enhance the amount of changes in the coordination polyhedron of Fe at T_g. However, the oxidized peralkaline haplogranitic sample shows no difference compared to the metaluminous haplogranitic sample despite the difference in polymerization. Thus, a certain polymerization threshold may have to be reached to cause detectable changes in the coordination polyhedron. Additionally, the presence of Al could have an inhibiting or delaying effect on the dynamics of the changes occurring in the supercooled liquid or close to T_g.

Farges et al. (1994) observed a coordination change around Ni^{2+} (isostructural to Fe^{2+}) between the glassy state and the melt in Na-disilicate glass, but none in more polymerized glasses and melts of anhydrous and hydrous NS3 and albite (Farges et al. 2001). In contrast, for the Fe^{2+}-dominated samples studied here, changes are observed for NS3 and also for the nominally polymerized haplogranite. This difference and the lack of a systematic relationship with the temperature-dependent bond valence of the

alkali cations of the system imply that the relationship between coordination changes in the melt and glass and NBO/T appears to be complex and element- or species-specific. Another possibility is that the observed changes in local environment around Fe are more or less decoupled from the bulk melt structure or even from the medium-range environment. It is not obvious whether the different behavior observed for the various elements might also reflect differences in the processes occurring in the temperature region close to T_g. In the case of Fe, the similarity of the observations for reduced and oxidized alkali-silicate compositions is striking, as the fairly large differences between the glass and the melt in the oxidized alkali-silicate compositions are quite unexpected. Only small, if any, changes around higher charged cations are likely (cf. Farges and Brown 1996). In this respect, the observed changes for Fe^{2+} can be considered as an adaptation of the local structure around Fe to changes in the bulk structure (similar to Ni^{2+} in Na-disilicate glass, Farges et al. 1994). In the case of the Fe^{3+}-dominated samples, one could try to relate the large differences between glass and melt to onset of ordering and crystallization, similar to the observations in experiments on the viscosity or crystallization of supercooled liquids of Fe^{3+}-dominated silicate melts (e.g., Richet et al. 1996; Burkhard 2001; Liebske et al. 2003). In these studies, a time dependence of the viscosity was observed that could be related to formation of Fe-oxides. However, formation of ordered domains or crystals would mean local enrichment of Fe atoms by diffusion, which is a relatively slow process and rather unlikely for the cooling rates used here.

The study presented here shows that all the XANES features have to be considered together, from the pre-edge feature to the first EXAFS oscillations to derive reliable information on geometry and speciation (oxidation state, interatomic distances). Combining all these information reveals that differences between glass and melt are detectable, but not as strong as suggested earlier (Waychunas et al. 1988; Jackson et al. 1993). With these results in mind, the local structural environment around Fe in glass may be still taken as a good approximation for the melt structure, provided the melt is quenched fast enough through the temperature interval of T_g. A parallel study on Fe in hydrous glass and melt has shown that the species found in such glasses can be affected significantly by the quench process, where the quench rates accessible near T_g were not sufficient to preserve the species present in the melt (Wilke et al. 2006).

ACKNOWLEDGMENTS

The support of E. Welter, K. Klementiev (HASYLAB) and A. Erko (BESSY) during beam time is highly appreciated. We thank B. Aichinger (Institute fur Mineralogie, Hannover) for her efforts in building the in-situ cell and D. Vollmer for help and advice in the wiring of the power and control units. We thank K. Grottke (HVB, Berlin) for providing the Tennolan-foil. We thank P. Czaja (Museum für Naturkunde, Berlin) and O. Appelt (GFZ Potsdam) for support during electron microprobe analysis. This study was supported by the Deutsche Forschungsgemeinschaft (DFG) through projects Wi-2000/1-1 and Wi-2000/1-2 and through the DAAD-EGIDE PROCOPE program. Reviews by Q. Liu and D. Dingwell are highly appreciated.

REFERENCES CITED

Alberto, H.V., Pinto da Cunha, J.L., Mysen, B.O., Gil, J.M., and Ayres de Campos, N. (1996) Analysis of Mössbauer spectra of silicate glasses using a two-dimensional Gaussian distribution of hyperfine parameters. Journal of Non-Crystalline Solids, 194, 48–57.

Ankudinov, A.L., Ravel, B., Rehr, J.J., and Conradsen, S.D. (1998) Real-space multiple scattering calculation and interpretation of X-ray absorption fine structure. Physical Review (B), 58, 7565–7576.

Attenkofer, K., Brüggmann, U., Haack, N., Herrmann, M., Kappen, P., and Welter, E. (2000) Improvements for absorption spectroscopy at beamlines A1, E4, X1. HASYLAB Annual Report, 63–68.

Berry, A.J., O'Neill, H.St.C., Jayasuriya, K.D., Campbell, S.J., and Foran, G.J. (2003) XANES calibrations for the oxidation state of iron in a silicate glass. American Mineralogist, 88, 967–977.

Bianconi, A., Dell'Ariccia, M., Gargano, A., and Natoli, C.R. (1983) Bond length determination using XANES. In A. Bianconi, L. Incoccia, and S. Stilpcich, Eds., EXAFS and Near Edge Structure, 27, p. 57–61. Springer Series in Chemistry and Physics, Berlin.

Bouhifd, M.A., Richet, P., Besson, P., Roskosz, M., and Ingrin, J. (2004) Redox state, microstructure and viscosity of a partially crystallized basalt melt. Earth and Planetary Science Letters, 218, 31–44.

Brese, N.E. and O'Keeffe, M. (1991) Bond-valence parameters for solids. Acta Crystallographica, B47, 192–197.

Brown, G.E., Jr., Farges, F., and Calas, G. (1995) X-ray scattering and X-ray spectroscopy studies of silicate melts. In J.F. Stebbins, P.F. McMillan, and D.B. Dingwell, Eds., Structure, dynamics and properties of silicate melts, 32, p. 317–410. Reviews in Mineralogy, Mineralogical Society of America, Chantilly, Virginia.

Brown, I.D. and Altermatt, D. (1985) Bond valence parameters obtained from a systematic analysis of the inorganic crystal structure database. Acta Crystallographica, B41, 244–247.

Bugaev, L., Farges, F., Rusakova, E., Sokolenko, A., Latokha, Ya., and Avakyan, L. (2005) Fe coordination environment in Fe(II) and Fe(III) containing glasses via the Fourier-transform analysis of Fe K-XANES. Physica Scripta, T115, 215.

Burkhard, D.J.M. (2000) Iron-bearing silicate glasses at ambient conditions. Journal of Non-Crystalline Solids, 275, 175–188.

——— (2001) Crystallization and oxidation of Kilauea basalt glass: Processes during reheating experiments. Journal of Petrology, 42, 507–527

Calas, G. and Petiau, J. (1983) Coordination of iron in oxide glasses through high-resolution *K*-edge spectra: Information from the pre-edge. Solid State Communication, 48, 625–629.

Chakraborty, S. (1995) Diffusion in silicate melts. In J.F. Stebbins, P.F. McMillan, D.B. Dingwell, Eds., Structure, dynamics and properties of silicate melts, 32, p. 411–503. Reviews in Mineralogy, Mineralogical Society of America, Chantilly, Virginia.

Dingwell, D.B. (1989) Shear viscosities of ferrosilicate liquids. American Mineralogist, 74, 1038–1044.

——— (1991) Redox viscometry of some Fe-bearing silicate melts. American Mineralogist, 76, 1560–1562.

Dingwell, D.B. and Brearley, M. (1988) Melt densities in the CaO-FeO-Fe_2O_3-SiO_2 system and the compositional-dependence of the partial molar volume of ferric iron in silicate melts. Geochimica et Cosmochimica Acta, 52, 2815–2825.

Dingwell, D.B. and Virgo, D. (1987) The effect of oxidation state on the viscosity of melts in the system Na_2O-FeO-Fe_2O_3-SiO_2. Geochimica et Cosmochimica Acta, 51, 195–205.

Erko, A., Packe, I., Gudat, W., Abrosimov, N., and Firsov, A. (2000) A Graded Crystal Monochromator at BESSY II. SPIE, 4145, 122–128.

Farges, F. (2001) Crystal chemistry of iron in natural grandidierites: an X-ray absorption fine-structure spectroscopy study. Physics and Chemistry of Minerals, 28, 619–629.

Farges, F. and Brown, G.E., Jr. (1996) An empirical model for the anharmonic analysis of high-temperature XAFS spectra of oxide compounds with applications to the coordination environment of Ni in NiO, γ-Ni_2SiO_4, and Ni-bearing Na-disilicate glass and melt. Chemical Geology, 128, 93–106.

Farges, F., Waychunas, G.A., Brown, G.E., Jr., Calas, G., and Galoisy, L. (1994) Structural transformation in Ni-bearing $Na_2Si_2O_5$ glass and melt. Geophysical Research Letters, 21, 1931–1934.

Farges, F., Brown, G.E., Jr, Navrotsky, A., Gan, H., and Rehr, J.R. (1996) Cooordination chemistry of Ti (IV) in silicate glasses and melts: III. Glasses and melts from ambient to high temperatures. Geochimica et Cosmochimica Acta, 60, 3055–3065.

Farges, F., Brown, G.E., Jr., and Rehr, J.R. (1997) Ti K-edge XANES studies of Ti coordination and disorder in oxide compounds: comparison between theory and experiment. Physical Review (B), 56, 1809–1819.

Farges, F., Brown, G.E., Jr., Petit, P.E., and Munoz, M. (2001) Transition elements in water-bearing silicate glasses/melts. Part I. A high-resolution and anharmonic analysis of Ni-coordination environments in crystals, glasses, and melts. Geochimica and Cosmochimica Acta, 65, 1665–1678.

Farges, F., Lefrere, Y., Rossano, S., Berthereau, A., Calas, G., and Brown, G.E., Jr. (2004) The effect of redox state on the local structural environment of iron in silicate glasses: a combined XAFS spectroscopy, molecular dynamics, and bond valence study. Journal of Non-crystalline Solids, 344, 176–188.

Galoisy, L., Callas, G., and Arrio, M.A. (2001) High-resolution XANES spectra of iron in minerals and glasses: structural information from the pre-edge region. Chemical Geology, 174, 307–319.

Giuli, G., Pratesi, G., Cipriani, C., and Paris, E. (2002) Iron local structure in

tektites and impact glasses by extended X-ray absorption fine structure and high-resolution X-ray absorption near-edge structure spectroscopy. Geochimica et Cosmochimica Acta, 66, 4347–4353.
Hannoyer, B., Lenglet, M., Dürr, J., and Cortes, R. (1992) Spectroscopic evidence of octhedral iron (III) in soda-lime silicate glasses. Journal of Non-Crystalline Solids, 151, 209–216.
Hazen, R.M. and Finger, L.W. (1982) Comparative Crystal Chemistry. Temperature, Pressure, Composition, and the Variation of Crystal Structure, 231 p. John Wiley and Sons, New York.
Hess, K.U., Dingwell, D.B., and Webb, S.L. (1995) The influence of excess alkalis on the viscosity of a haplogranitic melt. American Mineralogist, 80, 297–304.
Jackson, W.E., Mustre de Leon, J., Brown, G.E., Jr., Waychunas, G.A., Conradsen, S.D., and Combes, J.M. (1993) High temperature XAS study of Fe_2SiO_4: Evidence for reduced coordination of ferrous iron in the liquid. Science, 262, 229–233.
Jackson, W.E., Farges, F., Yeager, M., Mabrouk, P.A., Rossano, S., Waychunas, G.A., Solomon, E.A., and Brown, G.E. Jr. (2005) Multi-spectroscopic study of Fe(II) in silicate glasses: Implications for the coordination environment of Fe(II) in silicate melts. Geochimica and Cosmochimica Acta, 69, 4315–4332.
Krause, M.O. and Oliver, J.H. (1979) Natural widths of atomic K and L levels, K alpha X-ray lines and several KLL auger lines. Journal of Physical and Chemical Reference Data, 8, 329–338.
Lange, R.A. and Carmichael, I.S.E. (1990) Thermodynamic properties of silicate liquids with emphasis on density, thermal expansion and compressibility. In J. Nicholls and J.K. Russell, Eds., Modern methods of igneous petrology: Understanding magmatic processes, 24, p. 25–64. Reviews in Mineralogy, Mineralogical Society of America, Chantilly, Virginia.
Liebske, C., Behrens, H., Holtz, F., and Lange, R.A. (2003) The influence of pressure and composition on the viscosity of andesitic melts. Geochimica et Cosmochimica Acta, 67, 473–485.
Liu, Q. and Lange, R.A. (2006) The partial molar volume of Fe_2O_3 in alkali silicate melts: Evidence for an average Fe^{3+} coordination number near five. American Mineralogist, 91, 385–393.
Lytle, F.W., Greegor, R.B., Sandstrom, D.R., Marques, D.R., Wong, J., Spiro, C.L., Huffman, G.P., and Huggins, F.E. (1984) Measurement of soft X-ray absorption spectra with a fluorescence ion chamber detector. Nuclear Instruments and Methods in Physics Research Section A, 226, 542–548.
Mysen, B.O. (1988) Structure and properties of silicate melts, 354 p. Elsevier, Amsterdam.
Mysen, B.O., Virgo, V., Neuman, E.R., and Seifert, F.A. (1985) Redox equilibria and the structural states of ferric and ferrous iron in melts in the system CaO-MgO-Al_2O_3-SiO_2-Fe-O: relationships between redox equilibria, melt structure and liquid phase equilibria. American Mineralogist, 70, 317–331.
Natoli, C.R. (1983) Near edge absorption structure in the framework of the multiple scattering model. Potential resonance or barrier effects? In A. Bianconi, L. Incoccia, and S. Stilpcich, Eds., EXAFS and Near Edge Structure, 27, p. 43–56. Springer Series in Chemistry and Physics, Berlin.
Richet, P. and Bottinga, Y. (1995) Rheology and configurational entropy of silicate melts. In J.F. Stebbins, P.F. McMillan, D.B. Dingwell, Eds., Structure, dynamics and properties of silicate melts, 32, p. 67–93. Reviews in Mineralogy, Mineralogical Society of America, Chantilly, Virginia.
Richet, P., Lejeune, A.M., Holtz, F., and Roux, J. (1996) Water and the vicosity of andesite melts. Chemical Geology, 128, 185–197.
Rossano, S., Balan, E., Morin, G., Bauer, J.-Ph., Calas, G., and Brouder, Ch. (1999) ^{57}Fe Mössbauer spectroscopy of tektites. Physics and Chemistry of Minerals, 26, 530–538.
Rossano, S., Ramos, A., Delaye, J.-M., Creux, S., Filipponi, A., Brouder, C.H., and Calas, G. (2000) EXAFS and molecular dynamics combined study of CaO-FeO-$2SiO_2$ glass. New insights into site significance in silicate glasses. Europhysics Letters, 49, 597–602.
Seifert, F. and Olesch, M. (1977) Mössbauer spectroscopy of grandidierite, $(Mg,Fe)Al_3SiO_9$. American Mineralogist, 62, 547–553.
Stebbins, J.F. (1995) Dynamics and structure of silicate and oxide melts: nuclear magnetic resonance studies. In J.F. Stebbins, P.F. McMillan, D.B. Dingwell, Eds., Structure, dynamics and properties of silicate melts, 32, p. 191–246. Reviews in Mineralogy, Mineralogical Society of America, Chantilly, Virginia.
Stebbins, J.F. and Farnan, I. (1992) The effects of temperature on silicate liquid structure: a multi-nuclear, high temperature NMR spectroscopic study. Science, 255, 586–589.
Stephenson, D.A. and Moore, P.B. (1968) The crystal structure of grandidierite, $(Mg,Fe)Al_3SiBO_9$. Acta Crystallographica B, 24, 1518–1522.
Toplis, M.J. and Carroll, M.R. (1995) An experimental study of the influence of oxygen fugacity on Fe-Ti oxide stability, phase relations, and mineral-melt equilibria in ferro-basaltic systems. Journal of Petrology, 36, 1137–1170.
Virgo, D. and Mysen, B.O. (1985) The structural state of iron in oxidized vs. reduced glasses at 1 atm.: a ^{57}Fe Moessbauer study. Physics and Chemistry of Minerals, 12, 65–76.
Wang, Z., Cooney, T.F., and Sharma, S.K. (1993) High-temperature structural investigation of $Na_2O{\cdot}0.5\ Fe_2O_3{\cdot}3\ SiO_2$ and $Na_2O{\cdot}FeO{\cdot}3\ SiO_2$ melts and glasses. Contributions to Mineralogy and Petrology, 115, 112–122.
Waychunas, G.A., Apted, M.J., and Brown, G.E., Jr. (1983) X-ray *K*-edge absorption spectra of Fe minerals and model compounds: near edge structure. Physics and Chemistry of Minerals, 10, 1–9.
Waychunas, G.A., Brown, G.E. Jr., Ponader, C.W., and Jackson, W.E. (1988) Evidence from X-ray absorption for network-forming Fe^{2+} in molten alkali silicates. Nature, 350, 251–253.
Westre, T.E., Kennepohl, P., DeWitt, J.G., Hedman, B., Hodgson, K.O., and Solomon, E.I. (1997) A multiplet analysis of Fe *K*-edge 1s–3d pre-edge features of iron complexes. Journal of the American Chemical Society, 119, 6297–6314.
Wilke, M., Farges, F., Petit, P.-E., Brown, G.E., Jr., and Martin, F. (2001) Oxidation state and coordination of Fe in minerals: An Fe *K*-XANES spectroscopic study. American Mineralogist, 86, 714–730.
Wilke, M., Partzsch, G.M., Bernhardt, R., and Lattard, D. (2004) Determination of the iron oxidation state in basaltic glasses using XANES at the *K*-edge. Chemical Geology, 213, 71–87.
Wilke, M., Schmidt, C., Farges, F., Malavergne, V., Gautron, L., Simionovici, A., Hahn, M., and Petit, P.E. (2006) Structural environment of Fe in water-bearing silicate glass and melt—evidence from X-ray absorption spectroscopy. Chemical Geology, 229, 144–161.
Wu, Z.Y., Gota, S., Jollet, F., Pollak, M., and Gautier-Soyer, M. (1997) Characterization of iron oxides by x-ray absorption at the oxygen *K* edge using a full multiple-scattering approach. Physical Review B, 55, 2570–2577.
Wu, Z., Bonnin-Mosbah, M., Duraud, J.P., Métrich, N., and Delaney, J.S. (1999) XANES studies of Fe-bearing glasses. Journal of Synchrotron Radiation, 6, 344–346.

MANUSCRIPT RECEIVED MAY 3, 2005
MANUSCRIPT ACCEPTED JUNE 14, 2006
MANUSCRIPT HANDLED BY PAUL ASIMOW